Journal Homepage: -www.journalijar.com

INTERNATIONAL JOURNAL OF ADVANCED RESEARCH (IJAR)

Article DOI:10.21474/IJAR01/24480
DOI URL: http://dx.doi.org/10.21474/IJAR01/24480

ISSN (O): 2320-5407
ISSN (P): 3107-4928

RESEARCH ARTICLE

CONTRIBUTION OF AIRBORNEGEOPHYSICALIMAGING TO THE MAPPING OF BIRIMIAN FORMATIONS IN THE KALAMONMINING PERMIT, BOUNA, NORTHEASTERN CÔTE D'IVOIRE

Aboubakar Sidik Ouattara[1], Ayo Richmon Beugre[2] and Droh Laciné Goné[1]

1. Nangui ABROGOUA University, UFR of Environmental Sciences and Management, Geosciences and Environment Laboratory, 02 BP 801 Abidjan 02, Côte d'Ivoire.
2. Félix HOUPHOUET-BOIGNY University, UFR of Earth Sciences and Mineral Resources, Laboratory of Geology, Mineral and Energy Resources, 22 BP 582 Abidjan 22, Côte d'Ivoire.

Manuscript Info

Manuscript History
Received: 16 August 2026
Final Accepted: 18 September 2026
Published: October 2026

Key words:-
Aeromagnetics, Dykes, Petrography, Kalamon, Bouna, West African Craton.

Abstract

The Kalamon area, located within the Bouna mining district in northeas tern Côte d'Ivoire, forms part of the Paleoproterozoic domain of the Man Shield (West African Craton). In this sector, the presence of a subcontinuous and particularly thick lateritic cover (30 to 90 m) represe nts a major obstacle to direct geological mapping. This study combines high resolution airborne geophysical data processing (aeromagnetics an d gamma ray spectrometry) with detailed petrographic examination of core drill samples to map and characterize the dolerite dyke swarms traversing the Kalamon mining permit. Filtered analysis of the total magnetic field (reduction to the pole, analytic signal, and first vertical derivative) reveals narrow, highly magnetic linear anomalies with prefe rential N-S to NNE-SSW and NW-SE trends. Microscopic examination demonstrates that these basic intrusions exhibit a typical ophitic to subo phitic texture, dominated by interlocking plagioclase laths (labradorite to bytownite) and augite, accompanied by a significant proportion of iron titanium oxides (titaniferous magnetite and ilmenite), which accou nt for the high aeromagnetic response. Low-grade deuteric alterations are marked by partial uralitization of pyroxenes and sericitization of plagioclases. This integrated geophysical and petrographic approach proves highly effective in reconstructing subvolcanic magmatic conduit s and refining the regional geodynamic framework.

"© 2026 by the Author(s). Published by IJAR under CC BY 4.0. Unrestricted use allowed with credit to the author."

Introduction:-

In Precambrian cratons, and more particularly within the West African Craton, mafic dyke swarms (dolerites, gabbros, and sheeted basalts) constitute premier geodynamic markers (Milési et al., 1989; Ernst et al., 2013). They reflect major episodes of lithospheric extension, often associated with the breakup of supercontinents or the emplacement of large igneous provinces (LIPs) (Baratoux et al., 2011; Eglinger et al., 2017).In northeastern Côte d'Ivoire, the Bouna region—and more specifically the Kalamon mining permit—is characterized by a

Corresponding Author:-Aboubakar Sidik Ouattara
Address:-Nangui ABROGOUA University, UFR of Environmental Sciences and Management, Geosciences and Environment Laboratory, 02 BP 801 Abidjan 02, Côte d'Ivoire.

Paleoproterozoic basement (approximately 2.2–2.1 Ga) cut by multiple generations of brittle structures and dyke intrusions (Siagné et al., 2022). However, the geological study of these Birimian structures is strongly constrained by advanced lateritic weathering, which masks lithological contacts and outcrop continuity.To overcome these field constraints, high-resolution airborne geophysics—particularly magnetometry and gamma-ray spectrometry—constitutes a high-performing, non-destructive method for mapping lithological variations and the structural network beneath cover (Reford, 2006; Aïfa, 2021).The main objective of this work is to combine the results of airborne geophysical processing and petrographic analyses under a polarizing microscope to establish the structural mapping, dyke geometry, and mineralogical characterization of the dolerite dykes within the Kalamon permit.

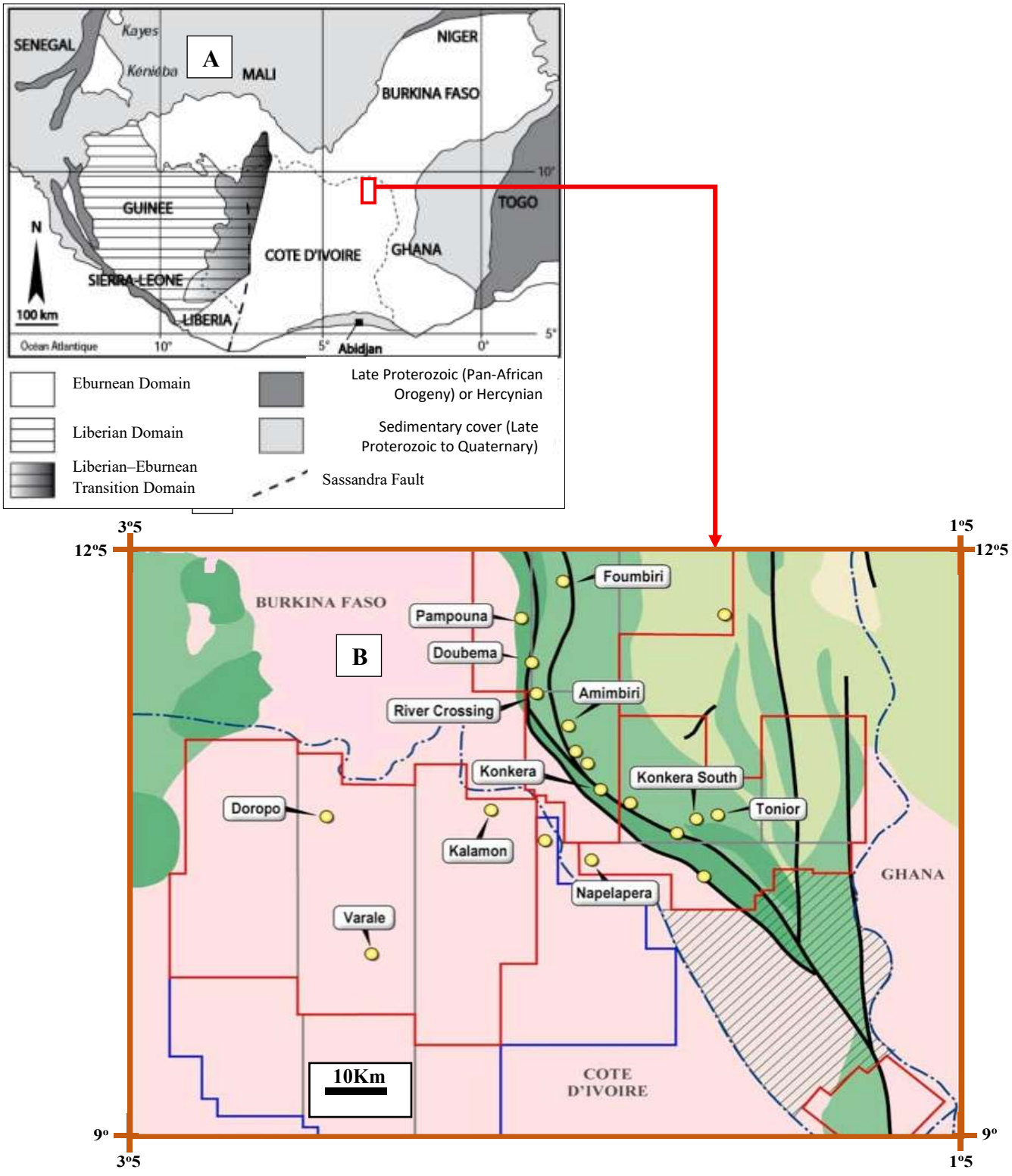
Regional and Local Geological Setting:-

The Kalamon mining permit is situated in the heart of the Paleoproterozoic Baoulé-Mossi domain (Fig. 1 A), which forms most of the eastern and central parts of the West African Craton in Côte d'Ivoire (Tagini, 1971 ; Bessoles, 1977). The architecture of this Precambrian basement is the product of the Eburnean orogeny (2.2–2.0 Ga), characterized by major episodes of crustal accretion, subduction, and tectono-metamorphic collision (Boher et al., 1992 ; Feybesse et al., 2006 ; Baratoux et al., 2011).

On a regional scale, this crystalline and crystallophyllian basement is mainly structured by two major lithotectonic assemblages. On the one hand, the volcano-sedimentary greenstone belts (Birimian), formed between 2.15 and 2.10 Ga, comprise mafic lava sequences dominated by tholeiitic basalts, intermediate-to-fclsic flows, and volcano-sedimentary deposits (detrital sediments and tuffs). These sequences have recorded polyphase regional metamorphism with an intensity generally ranging from green-schist to lower amphibolite facies (Hirdes et al., 1996 ; Lompo, 2009). On the other hand, the syn- to post-orogenic granitoid plutonic complexes, which intrude and frame these greenstone belts, are dominated by tonalite-trondhjemite-granodiorite (TTG) suites as well as potassic calc-alkaline granites (Kouamelan et al., 1997 ; Gasquet et al., 2003 ; Martin et al., 2005).

On a local scale, the Kalamon area is characterized by a heterogeneous granitoid basement (Fig. 1 B) dissected by a dense network of brittle to brittle-ductile faults and shear corridors with a preferential N-S to sub-N-S orientation. These zones of crustal weakness played a key hydrogeological and structural role by acting as preferential conduits (drains) for the ascent and injection of late tholeiitic magmas, which crystallized as dolerite dyke swarms (Dadet, 1969 ; Siagné et al., 2022 ; Siagné et al., 2025).

Finally, the morphology and outcrop conditions of this area are strongly controlled by intense, prolonged supergene weathering under a humid tropical climate. This weathering dynamic promoted the development of a duricrust profile and a thick ferruginous and bauxitic lateritic cover frequently reaching 50 to 90 meters in depth. This thick regolith almost completely masks lithological contacts at the surface, making the combined use of core drilling and airborne geophysical imaging essential to accurately reconstruct the fine geometry of the geological structures.


A
SENEGAL
Kayes
Kenieba
MALI
NIGER
BURKINA FASO
GUINEE
TOGO
COTE D'IVOIRE
GHANA
SIERRA LEONE
LIBERIA
N
100 km
Océan Atlantique
10°
5°
0°
Abidjan
Eburnean Domain
Liberian Domain
Liberian–Eburnean Transition Domain
Late Proterozoic (Pan-African Orogeny) or Hercynian
Sedimentary cover (Late Proterozoic to Quaternary)
Sassandra Fault
B
3°5
1°5
12°5
9°
BURKINA FASO
Foumbiri
Pampouna
Doubema
Amimbiri
River Crossing
Konkera
Konkera South
Tonior
Doropo
Kalamon
Napelapera
Varale
GHANA
COTE D'IVOIRE
10Km

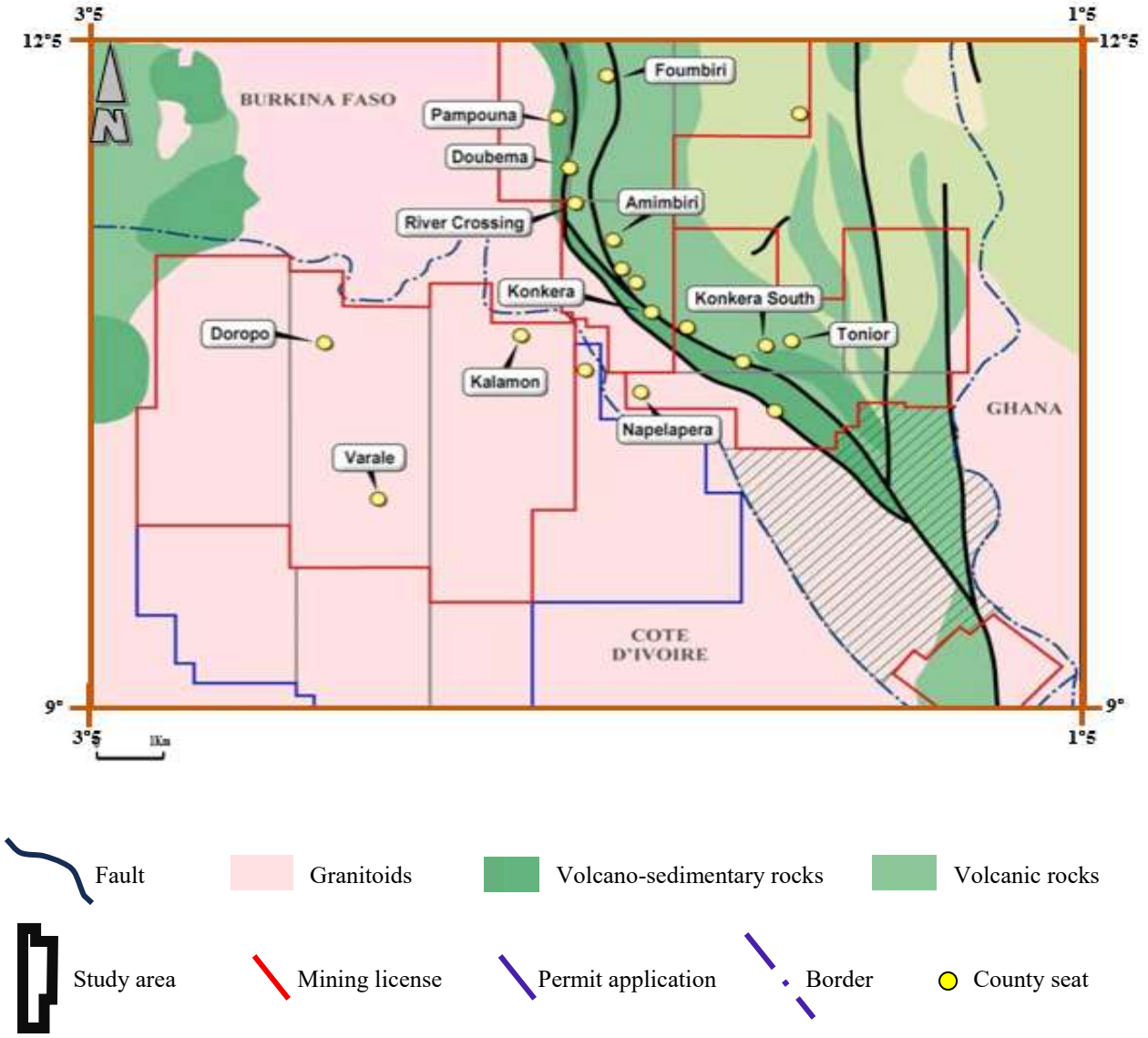


Figure 1 : (A) Map of the Man Rise (Bessoles, 1977 ; modified) and (B) Synthetic geological map of the Kalamon mining sector (CENTAMIN Report, 2017).

Methodology:-

Airborne geophysics:-

Airborne geophysical surveys constitute a rapid, large-scale reconnaissance approach, particularly well-suited for covering extensive areas prior to refining the interpretation through detailed investigations. In this study, the airborne surveys were conducted using a magnetometer and a spectrometer onboard an aircraft, enabling the simultaneous acquisition of magnetic field variations and gamma-ray radioactivity. The airborne geophysical data used originate from a high-resolution regional survey acquired along flight lines spaced 200 m apart, with a sampling interval of 5 m along profiles and a nominal flight height set at 80 m.**3-**

Magnetism:-

The magnetic method measures spatial variations in the intensity of Earth's magnetic field, which are influenced by global contributions from the core and mantle as well as magnetic susceptibility contrasts of local geological bodies. Measurements were collected using a cesium vapor magnetometer featuring a sampling rate of 0.1 seconds and a high resolution of 0.01 nT. Raw data processing required applying the Reduction to the Pole (RTP) correction to position magnetic anomalies directly above their geological sources by overcoming local inclination effects. To optimize structural and lithological mapping, additional enhancements were applied, including the first vertical derivative (1VD), which highlights vertical gradients and sharpens the boundaries of geological bodies and

subvertical contacts, and the analytical signal (AS), which simplifies magnetic source geometry by generating positive anomalies centered over inductive bodies.

Radiometry (RAD):-

Airborne gamma-ray spectrometry maps the superficial distribution of natural radioelements (potassium [K], thorium [Th], and uranium [U]). The equipment included a spectrometer equipped with thallium-activated sodium iodide (NaI) crystals capable of measuring energy spectra associated with the radioactive decay of these tracer elements.

Ground Validation and Petrographic Analyses:-

The interpretation of geophysical data was validated by a rigorous field campaign relying on reference cartographic documents. Due to the thick supergene weathering cover (reaching 50 to 90 m in thickness depending on the sector), direct surface observations were complemented and supplemented by the systematic analysis of core boreholes.Sample selection was based on a meticulous analysis of lithological logs in order to select the freshest, most homogeneous, and representative facies reflecting lateral and vertical continuity. A total of around one hundred samples were collected in compliance with geological safety standards. The positions of outcrops and boreholes were geolocated using a Garmin Etrex GPS receiver.The petrographic and mineralogical study began with a macroscopic visual description of the various lithologies before proceeding to microscopic analysis using a polarizing microscope. The latter relied on the examination of about twenty thin sections, prepared in part at the University of Paris XI (France) and at the Analysis and Research Center (CAR) of the Petroleum Operations Company of Côte d'Ivoire (PETROCI). All of these macroscopic and microscopic descriptions were carried out at the Laboratory of Geology, Mineral Resources, and Energy of the UFR of Earth Sciences and Mineral Resources at Université Félix Houphouët-Boigny in Abidjan-Cocody. Additionally, the magnetic susceptibility of the samples was measured using a KT-10 magnetic susceptibility meter from Terra Plus (Fig. 2).



Figure 2 : KT-10 Magnetic Susceptibility Meter.

Computer Processing and Cartographic:-

Integration The computational methodology relied on the multi-layer integration of geophysical data (magnetism and radiometry) and geological mapping using the Quantum GIS (QGIS) Geographic Information System. The extraction of lineaments from the 1VD aeromagnetic geophysical image enabled the generation of a detailed magnetic discontinuity map. In contrast, major lineaments were highlighted using reduced-to-the-pole (RTP) magnetic data. Measurements were plotted on stereograms using Georient software. Existing 1:200,000 geological and 1:50,000 topographic maps were georeferenced in the UTM projection system (Zone 30N, WGS 84 Datum). Applying a cross-transparency (around 50%) between the aeromagnetic and radiometric survey images superimposed on the base map allowed for the generation of composite maps. This synoptic visual approach greatly

facilitates the identification of major structural lineaments, hidden faults, and major lithological contacts masked by the lateritic cover.

Results:-

Geological Mapping:-

The cross-referencing of airborne magnetic geophysical data with analytical signal processing (MAG-AS), radiometric data (RAD) (Fig. 3), and field lithological data (Figs. 4 and 5) enabled us to observe three distinct petrographically defined units that are unevenly distributed across the entire Kalamon permit (Fig. 6).

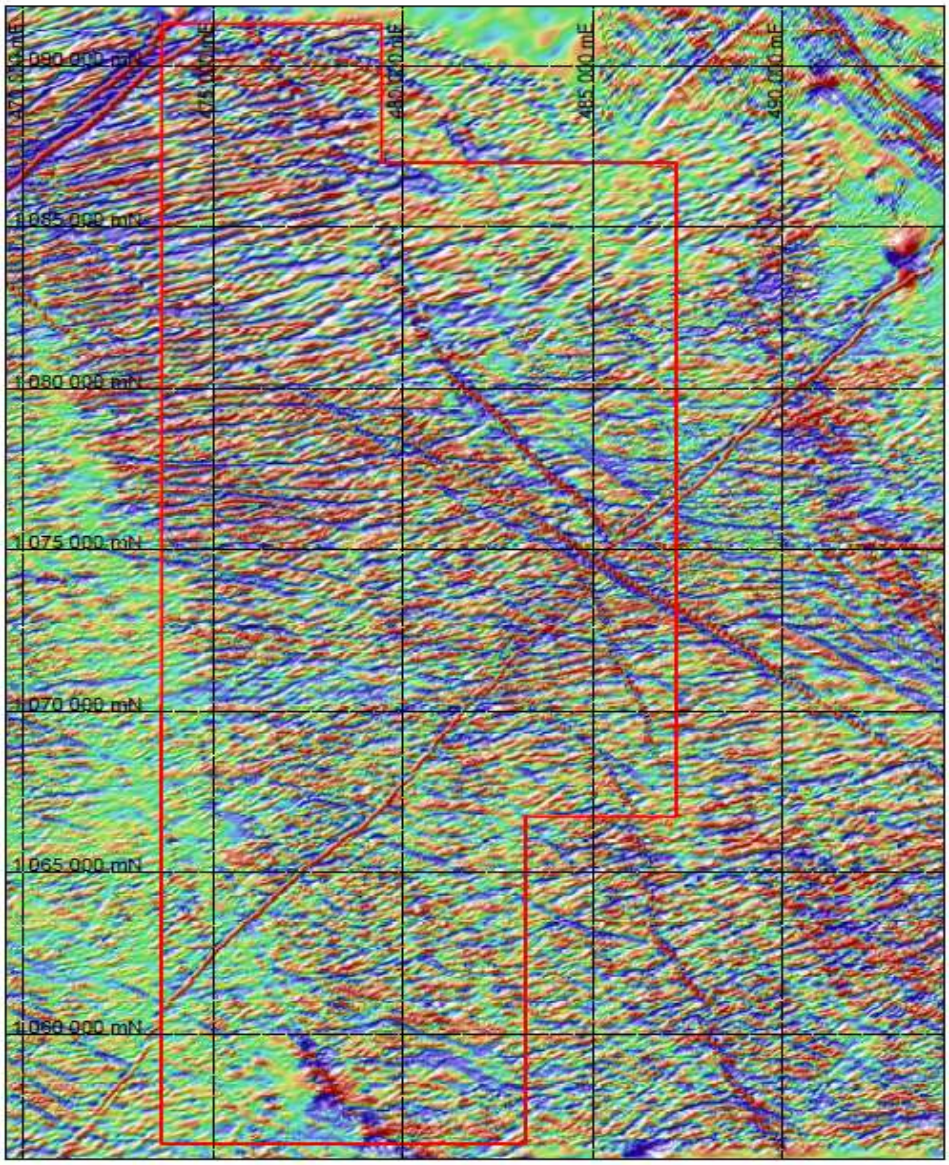


Figure 3 : 1VD-RTP TMI Geophysical Map.

Unit I (Undeformed Granodiorite):-

This unit, or Type I granodiorite, composed of undeformed or weakly deformed granodiorite, displays a slightly rough texture on the geophysical image, with magnetic susceptibilities ranging from 1.89 to 3.84 × 10^{-3} SI and a density varying from 2.54 to 2.74 × 10^{3} kg/m³, appearing in a yellowish-green tone (Table I). It appears to be in sharp contact with Unit II. In the Kalamon sector, undeformed granodiorites constitute a significant portion of the plutonic complexes. At the macroscopic scale, these rocks present a massive, mesocratic aspect with a pinkish or whitish tendency, possessing a medium- to coarse-grained granular texture. They display a visible mineralogy

dominated by translucent quartz, abundant feldspaths (plagioclases and potassium feldspaths), as well as disseminated biotite flakes (Fig. 4 A). Microscopic examination under polarized light accurately characterizes the primary mineral paragenesis and the deuteric alteration stages affecting these facies :

- **Quartz :** It represents 35 to 45% of the rock and occurs as large xenomorphic crystals with lobed boundaries, as well as clusters of interstitial micro-grains. The quartz frequently exhibits pronounced undulatory extinction, reflecting post-crystallization tectonic stresses experienced by the basement (Fig. 4 B).
- **Potassium feldspaths :** Largely dominated by orthoclase and microcline, they constitute 25 to 30% of the mineralogical volume. They manifest as large subhedral phenoblasts sometimes displaying Carlsbad twinning or a fine perthite network (albite exsolution), and are moderately altered by sericitization (Fig. 4 B).
- **Plagioclases :** More discreet than in the granodiorites, they represent 15 to 20% of the rock. Of sodic composition (oligoclase to albite), they occur as subhedral laths showing polysynthetic albite twins often blunted by secondary alteration (Fig. 4 B). A fine albitic rim or discrete zoning is frequently observed.
- **Biotite :** The main yet sparse ferromagnesian phase (3 to 6%), it occurs as fine subhedral lamellae of brown to greenish color, affected by partial chloritization. It contains zircon inclusions characterized by dark pleochroic haloes (Fig. 4 B).
- **Accessory and secondary minerals:** The accessory assemblage includes rare crystals of sphene, apatite, and disseminated opaque oxides. Low-grade hydrothermal alteration phases result in the development of sercite at the core of feldspaths, chlorite at the expense of biotite, and epidote microcrystals scattered throughout the matrix (Fig. 4 B).

Unit II (Deformed Granodiorite):-

It corresponds to the most extensive and dominant lithological unit of the Kalamon permit. This unit, corresponding to deformed or Type II granodiorites, exhibits a rough texture on the geophysical image, with a magnetic susceptibility ranging from 1.30 to 9.76 × 10^{-3} SI and a density varying from 2.54 to 2.69 × 10^{3} kg/m³. It appears in a red-to-dark-blue coloration associated with haloed yellow to sky-blue tones (Table I). This unit appears to intrude Unit I. The images indicate an unusual abrupt change between Unit II and Unit I, which undoubtedly corresponds to a lithological contact. Macroscopically, the granodiorites have a medium- to coarse-grained granular texture, darker mesocratic than that of Unit I, with a massive appearance. It is mainly composed of feldspars and quartz in variable proportions. These minerals are associated with biotite and amphibole, also in variable proportions (Fig. 4 C).

From a microscopic standpoint, the following minerals are observed:-

- Plagioclases : They are the most widely represented minerals (approximately 45 to 50%). The plagioclases are of highly variable size, euhedral, and altered. They exhibit polysynthetic twins often obliterated by alteration. The plagioclases present large, slightly sericitized areas (Fig. 4 D). Some plagioclases are zoned with a generally altered calcic core and a more or less clear albitic rim.
- Quartz : Quartz reaches proportions of 30 to 35% of the rock. It occurs as globular crystals and xenomorphic areas. This mineral displays highly variable sizes ranging from micro-grain to coarse grain with remarkable undulatory extinction (Fig. 4 D).
- Biotite : Accounting for 10 to 15%, biotite occurs as subhedral to euhedral lamellae, brown in color turning sometimes to light green, undoubtedly due to chloritization. It displays direct pleochroism. A few zircon inclusions surrounded by a dark halo are also observed (Fig. 4 D).

Unit III (Dolerite Dykes)

This unit, the youngest, corresponds to intermediate rock dykes cutting across the previous units. Their magnetic susceptibilities vary from 2.11 to 7.18 × 10^{-3} SI (strong response) with a density varying from 2.56 to 2.99 × 10^{3} kg/m³. They appear in a red coloration (Table I). Macroscopically, the Kalamon dolerites are dark, melanocratic to mesocratic rocks, very dense and little altered at depth (Fig. 5 A).

Under the microscope, the rocks display a remarkable ophitic to subophitic texture:-

- Plagioclases : They form (45–55%) entangled euhedral laths showing polysynthetic albite twinning. They are moderately affected by sericitization (Fig. 5 B).
- Pyroxenes: Represented predominantly by colorless to slightly greenish augite (30–40%), occupying the interstitial spaces between plagioclase laths. Some crystals show borders transformed into actinolite/tremolite (uralitization) (Fig. 5 B).

- Opaque minerals: They appear as disseminated skeletal or idioblastic grains (5–10%). Reflected-light analysis confirms the predominance of titaniferous magnetite and ilmenite. It is this high content of magnetic opaque minerals that explains the intense signature observed on airborne surveys (Fig. 5 B).
- Accessory and secondary minerals: Traces of apatite, late interstitial quartz, chlorite, and epidote associated with hydrothermal-deuteric alteration.

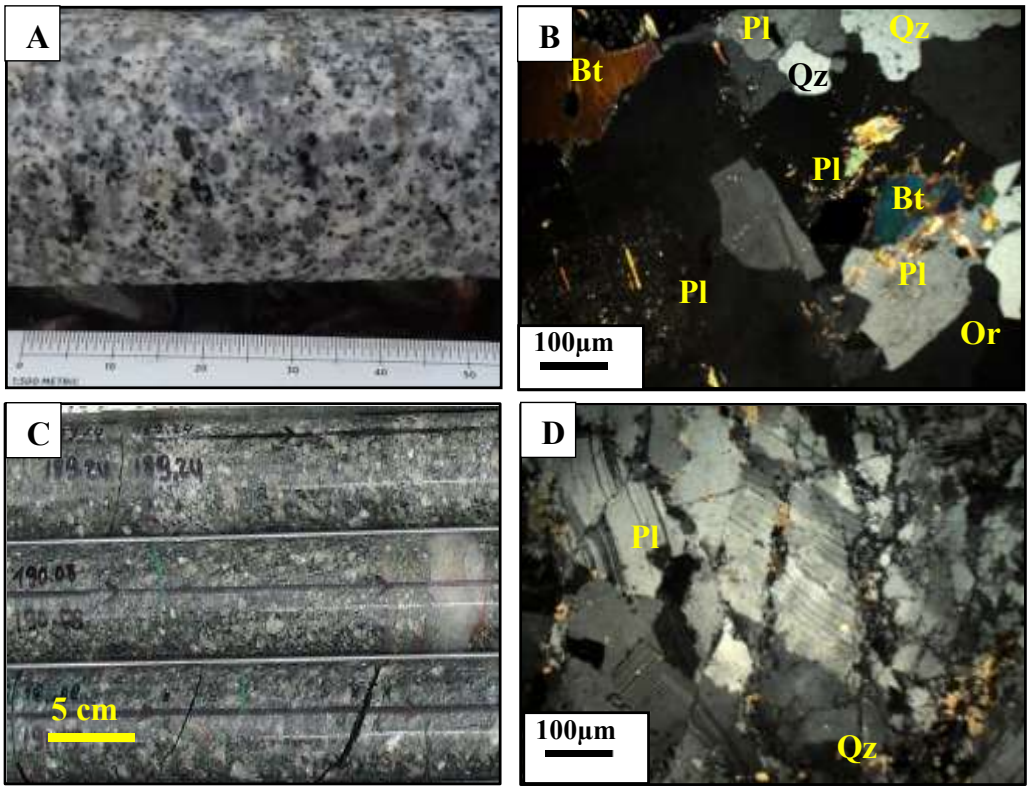


Figure 4 : Macroscopic aspects and photomicrograph of a granodiorite.

A : Granite coresample **; B :** Photomicrograph of the granite**.**
Pl : plagioclase ; Qz : quartz ; Or : orthoclase ; Bt : biotite ; Hbl : green hornblende ; Ep : epidote ; Ser : sericite

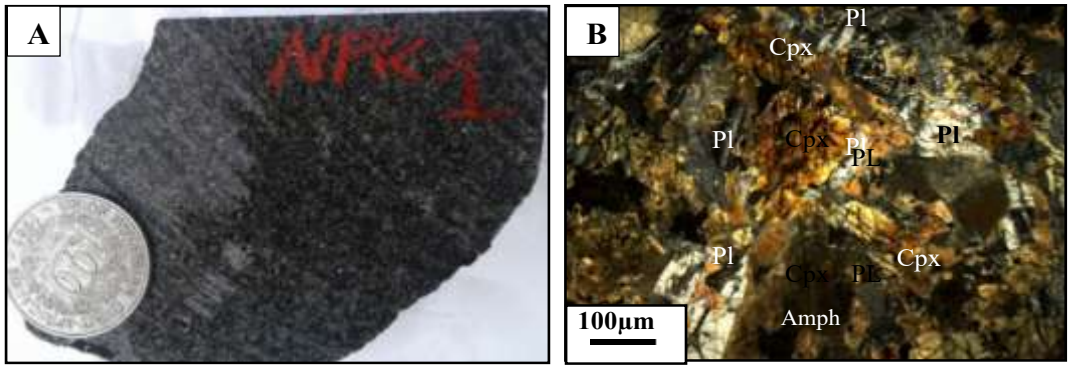
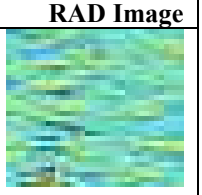
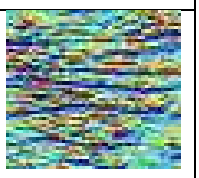
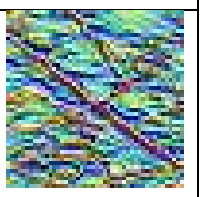


Figure 5 : Macroscopic aspect and photomicrograph of a dolerite.
A : Macroscopic aspect of a dolerite ; **B :** Photomicrograph of the diorite.
Pl : plagioclase ; Cpx : clinopyroxene ; Bt : biotite ; Amph: amphibole ; Op : opaque mineral

Table I : Characteristic color set for lithologies.

Unit	Lithology	Magnetic Susceptibility (SI)	Characteristics	TMI 1VD-RTP + RAD Image
I	Undeformed Granodiorite	1,89 et 3,84 10^{-3}	- Slightly rough texture - Low magnetic response	
II	Deformed Granodiorite	1,30-9,76 10^{-3}	- Strongly rough texture - High magnetic response	
III	Dolerite Dykes	2,11-7,18 10^{-3}	- Linear structure - High magnetic response	

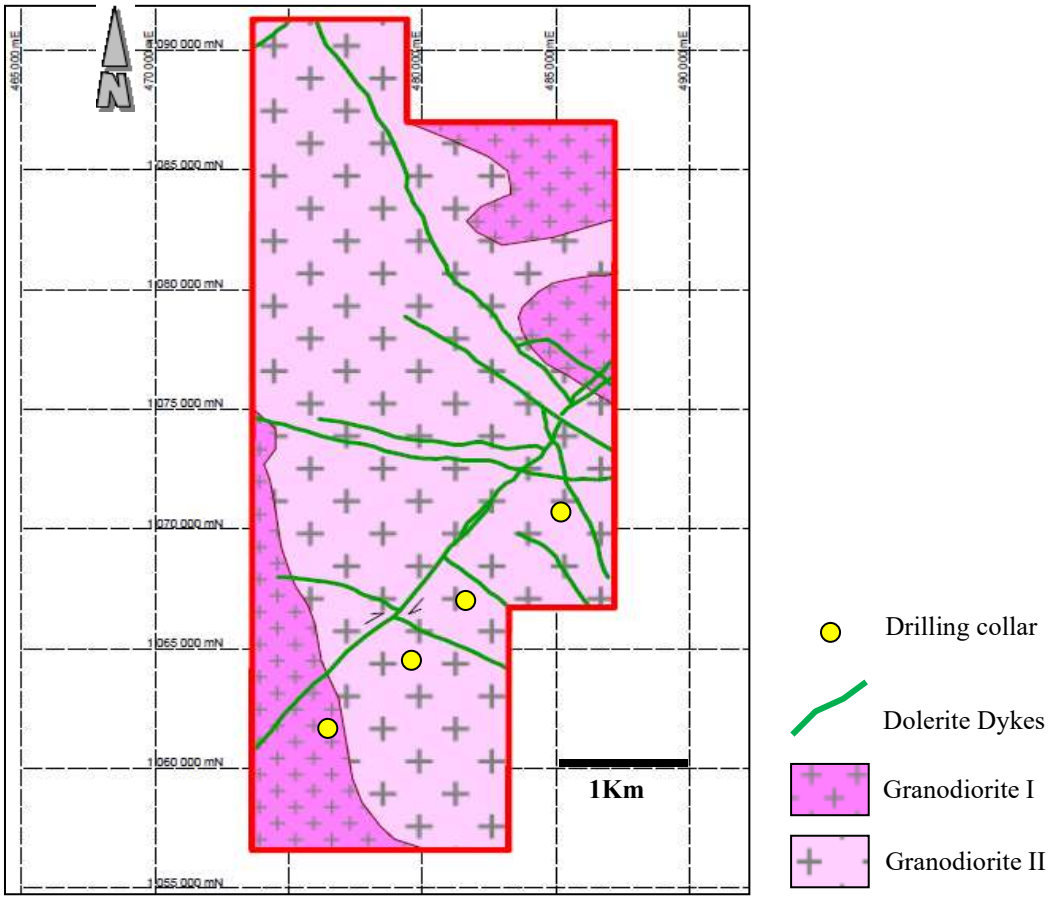


Figure 6 : Geological sketch of the study area based on geophysical and field data.

Structural Analysis:-

Visual and manual interpretations of the geophysical images (Fig. 7) enabled us to obtain a lineament map (Fig. 8). This mapping was complemented by studies carried out on drill cores, which allowed us to identify several families of lineaments.

Lineament Map:-

The lineament data maps (Fig. 7) generally show linear structures, commonly interpreted in granitoids as related to fracturing, jointing, foliation, banding, or schistosity. The extracted lineaments (Fig. 8) vary in length from the metric to the plurikilometric scale. Their distribution across the image follows several orientations. Statistical analysis of the lineaments reveals three major families of lineament orientations. Based on the number of lineaments extracted from the 1VD-RTP TMI image and discriminated by a threshold greater than 10%, we can observe on the directional rose diagram (Fig. 9) that the NE–SW lineament class ranging between [N30°–N70°] is the most abundant. The second directional class is the NW–SE direction, represented by the [N110°–N130°] class. Finally, the third lineament class is globally oriented E–W [N080°–N100°]. Indeed, the major NE, NW, and E–W lineaments define a fracture system resulting from ductile-brittle deformation.

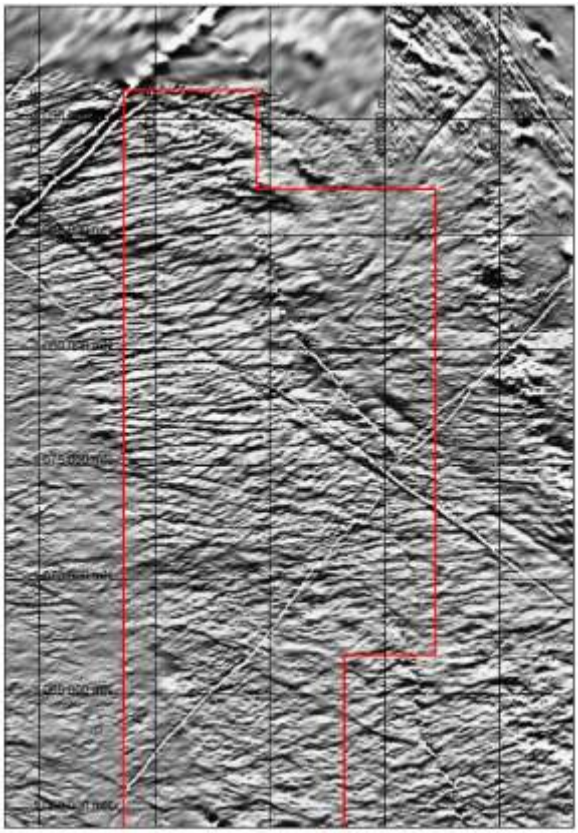


Figure 7 : TMI 1VD-RTP image showing lineaments.

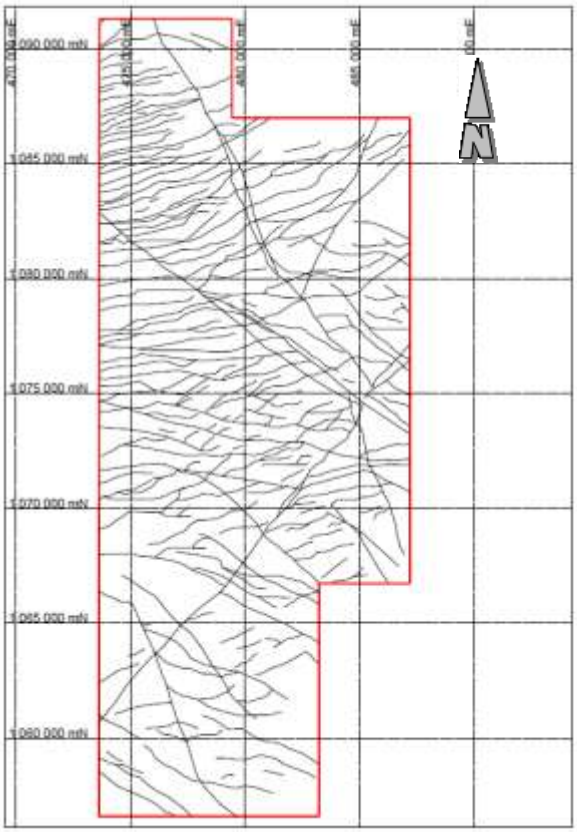
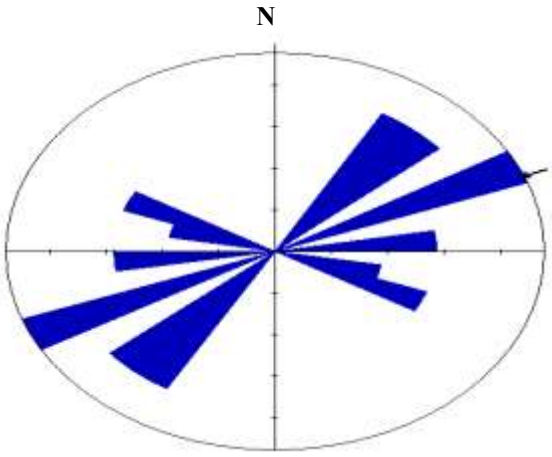


Figure 8 : Lineament network map.



Ground Work Validation:-

Outcrop Observations:-

In the field, structural elements were difficult to measure due to intense weathering, which renders outcrops nearly invisible. Nevertheless, we were able to take a few measurements (Fig. 10) that confirm structures belonging to the [N120°–N130°] directional class.

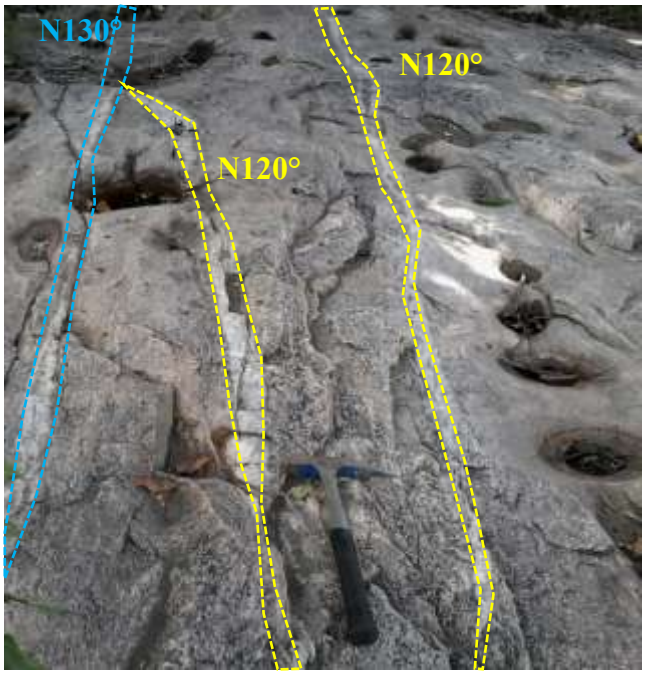


Figure 10 : Photograph illustrating a granite outcrop with N130°-trending fractures filled with milky quartz.

On Drill Cores:-

Diamond drilling campaigns also intersected type I and II granodiorites as well as dolerite d

Several families of mesostructures were identified on the drill cores. These structures result from brittle tectonics and consist of quartz veins and veinlets, as well as fractures.

- **Veins and Veinlets:-**

Quartz veins can be grouped into several families with specific geometric characteristics (thickness, strike, and dip). The veins range in thickness from a few centimeters to several meters. As for veinlets, whose thickness is less than 1 cm, they are predominant in the study area. They constitute a true network of fractures filled with quartz crystals (Fig. 11 A), sometimes associated with calcite, but they can also be infilled with chlorite, epidote, and hematite.

Measurements carried out on these structures reveal that they are pluridirectional (Fig. 11 B). Nevertheless, three main orientations emerge:

- NW–SE with dips toward the SW (mean plane N130°, 45°SW);
- NE–SW with dips toward the NW (mean plane N40°, 35°NW); and
- the presence of sub-meridian N–S veins (mean plane N5°, 10°NW).

- Fractures

Fractures (sensu stricto) are widely observed in the cores (Fig. 11 C). These fractures are pluridirectional (Fig. 11 D) and crosscut the entire rock mass. Most measurements yield the following orientations:-

- NE–SW dipping toward the NW (mean plane N60°, 50°NW);
- N–S dipping toward the W (54°W);
- E–W dipping toward the SW (mean plane N280°, 35°NW).

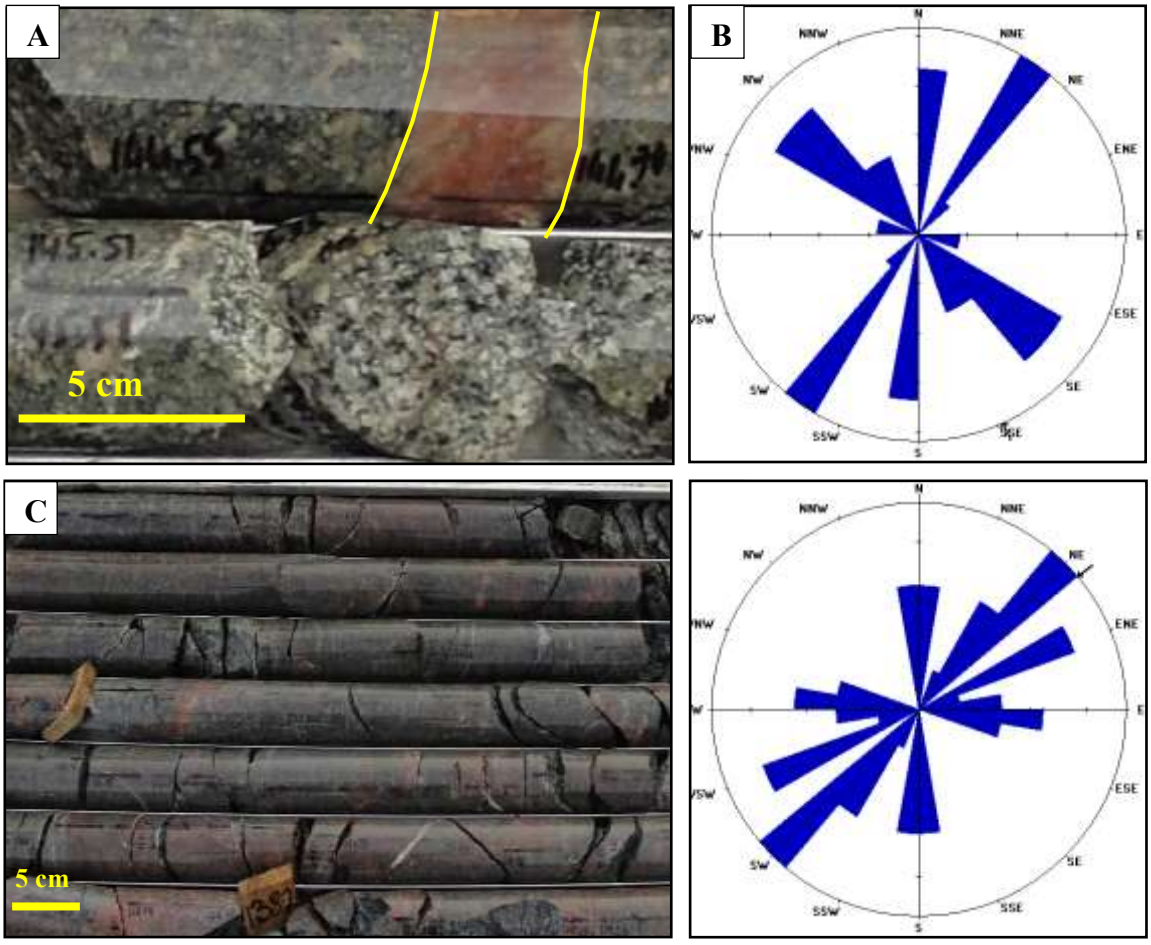


Figure 11 : Rose diagrams and photographs of some structures observed on drill core.

A : Directional rose diagram of quartz veins ; **B :** Photograph of a quartz vein **; C :** Directional rose diagram of fractures ; **D :** Photograph of fractures**.**

Discussion:-

Integration of Geophysical and Petrographic Data : Origin of Magnetic Signatures :-

Combining airborne geophysical imaging data (TMI 1VD-RTP and Analytic Signal) with petrographic and lithological observations highlights a close correlation between magnetic susceptibility contrasts and the nature of the intrusive facies. The undeformed granodiorites (Unit I) are characterized by a weak to moderate magnetic response and a slightly rough texture. Mineralogically, this is explained by the abundance of felsic silicate phases (quartz and feldspars totaling over 75–80%) and the scarcity of primary iron oxides, with biotite and green hornblende constituting the bulk of the ferromagnesian minerals. In contrast, the deformed Type II granodiorites and especially the dolerite dykes (Unit III) are distinguished by sharp, high-amplitude internal magnetic anomalies and a strongly rough texture. Micrographic examination of the dolerites demonstrates that this high magnetic intensity is directly linked to the presence of 5% to 10% primary opaque minerals, dominated by titaniferous magnetite and ilmenite disseminated within an ophitic to subophitic texture matrix (augite and plagioclase). These observations corroborate the works of Reford (2006) and Airo &Loukola-Ruskeeniemi (2004), who emphasize that magnetic susceptibility variations in crystalline basements are primarily governed by the distribution of opaque oxides and deuteric alteration parageneses (uralitization and saussuritisation).

Structural Control and Kinematics of Magmatic Intrusions :-

Statistical analysis of the lineaments extracted from the TMI 1VD-RTP image and the rose diagram (Fig. 9) reveal major structuring dominated by the N120°–N130° direction, composed of secondary families oriented N080°–N100° and N030°–N040°. Although the thick supergene weathering cover (often exceeding 50 meters) almost entirely masks surface outcrops a classic constraint documented in the West African basement (Tagini, 1971 ; Bessoles, 1977), validation by diamond drilling and rare field observations (multimeter-scale N130°-trending fractures filled with milky quartz) confirm the primary role of these tectonic corridors. These fracture families and shear zones constitute major crustal structures inherited from the Eburnean orogeny. They acted as preferential hydrogeological and magmatic pathways, favoring on the one hand the ascent and late emplacement of Type II granites, and on the other hand the subsequent injection of tholeiitic magmas as dolerite dykes (Dadet, 1969 ; Siagné et al., 2022 ; Siagné et al., 2025).

This brittle to brittle-ductile tectonic regime reflects a classic post-orogenic extensional or transtensional setting in the geodynamic evolution of the West African Craton (Dumont et al., 1997 ; Ernst et al., 2013). The petrological association observed in the Kalamon sector, combining an intrusive granodioritic basement and a late swarm of intermediate dykes, fits harmoniously into the regional geodynamic framework of the Paleoproterozoic Baoulé-Mossi domain (Boher et al., 1992 ; Feybesse et al., 2006). On a regional scale in Côte d'Ivoire, the Kalamon Type I and II granodiorites share strong petrographic affinities with plutonic complexes described in other Ivorian greenstone belts, such as Fettékro, Oumé, or Dabakala (Doumbia et al., 1998 ; Gnanzou, 2014 ; Allibro et al., 2014). In this context, the presence of amphibole phases (green hornblende) and biotite affected by low-grade hydrothermal alteration (chloritization, epidotization, and sericitization) constitutes a ubiquitous feature of peri-intrusive halos and mineralized corridors of the Ivorian Birimian (Milési et al., 1989 ; Kouadio et al., 2023). Finally, across the West African Craton scale, the N120°- and N–S-oriented dolerite dyke swarms crosscutting the Eburnean granitoids reflect regional lithospheric fracturing phases comparable to those recognized in Burkina Faso (Lompo, 2009 ; Vidal et al., 2009) and Ghana (Hirdes et al., 1996 ; Allibone et al., 2002). These basic intrusions generally seal the end of the major tectono-metamorphic paroxysms of the Eburnean orogeny (2.1–2.0 Ga) and bear witness to major continental extensional events preceding the final stabilization of the craton (Baratoux et al., 2011 ; Eglinger et al., 2017).

Conclusion:-

This study carried out on the Kalamon mining permit (Bouna region, northeastern Côte d'Ivoire) demonstrates the efficiency and relevance of the methodological approach coupling high-resolution airborne geophysical imaging and in-depth petrographic analysis on drill cores. In a Paleoproterozoic basement context heavily masked by a thick supergene weathering cover (laterites and saprolites reaching depths of 50 to 90 meters), aeromagnetic data processing—including Reduction to the Pole (RTP), the First Vertical Derivative (1VD), and Analytic Signal (AS)—overcame field constraints to map the structural architecture and spatial footprint of mafic dyke swarms with unprecedented precision. Petrographic and mineralogical investigations characterized these intrusions as dolerites with an ophitic to subophitic texture, dominated by the association of calcic plagioclases (labradorite to bytownite) and clinopyroxenes (augite), supplemented by a significant proportion of primary opaque minerals (titaniferous magnetite and ilmenite). It is precisely this abundance of iron-titanium oxides that justifies the intense linear

magnetic signature recorded by the airborne surveys. Structurally, statistical analysis of lineaments and major directions highlights rigorous tectonic control characterized by fault and dyke families with dominant N–S to NNE–SSW and NW–SE orientations (with a marked relay represented by the N120°–130° class). These crustal weakness corridors, inherited from the Eburnean orogeny, acted as major magmatic conduits during post-orogenic extensional phases. This dynamic fits perfectly into the regional geodynamic framework of the Baoulé-Mossi domain and the West African Craton, confirming the strategic interest of these magmatic markers for understanding the Precambrian lithosphere.

References:-

1. Aïfa, T. (2021). Geophysics and geodynamics of West African Craton. Journal of African Earth Sciences, 175, 104120.
2. Airo, M. L., &Loukola-Ruskeeniemi, K. (2004). Characterization of geological materials by magnetic and petrophysical properties: Application to ore exploration in Fennoscandia. Geological Survey of Finland, Special Paper, 37, 33–45.
3. Allibone, A., McCuaig, T. C., Harris, D., Etheridge, M., Munroe, S., Byrne, D., & Blenkinsop, J. (2002). Lower Proterozoic gold deposits in the Ashanti Belt, Ghana : Geochronological constraints. Economic Geology, 97(3), 505–517.
4. Allibro, A., Kouamé, F., & Yao, B. J. (2014). Pétrographie et contextegéodynamique des granitoïdes de la région de Dabakala (Nord-Est de la Côte d'Ivoire). Journal des Sciences Géologiques et Appliquées, 12(2), 45–60.
5. Baratoux, L., Jessell, M. W., Feybesse, J. L., Ilboudo, H., &Cottereau, N. (2011). Initiation and paleoproterozoic accretion of the West African Craton. Precambrian Research, 187(3-4), 169–199.
6. Bessoles, B. (1977). Géologie de l'Afrique : le Craton Ouest-Africain. Mémoires du BRGM, n° 88, Paris, 383 p.
7. Boher, M., Abouchami, W., Michard, A., Albarède, F., & Arndt, N. T. (1992). Crustal growth in West Africa at 2.1 Ga. Journal of Geophysical Research, 97(B1), 345–369.
8. CENTAMIN (2017) : Rapport technique de decembre 2017 du projet de Kalamon, Côte d'Ivoire, 20 p
9. Dadet, P. (1969). Notice explicative de la carte géologique de la République de Côte d'Ivoire au 1/500 000. SODEMI, Abidjan, 145 p.
10. Doumbia, S., Yao, B. J., Tagini, B., &Kouamé, F. (1998). Le magmatismepaléoprotérozoïque du sillon de Fettékro. Journal of African Earth Sciences, 27(3), 345–362.
11. Dumont, J. F., Poupinet, G., & Soule, J. C. (1997). Late Eburnean tectonic evolution of the West African Craton in Côte d'Ivoire. Precambrian Research, 84(1-2), 45–65.
12. Eglinger, A., Bari, A., Robb, L. J., Augenstine, M., & Zeh, A. (2017). Paleoproterozoic crustal evolution and gold metallogeny of the West African Craton. Ore Geology Reviews, 81, 1050–1068.
13. Ernst, R. E., Bleeker, W., Söderlund, U., & Kerr, A. C. (2013). Giant dyke swarms and mantle plumes: Implications for continental breakup. Geological Society, London, Special Publications, 382(1), 1–45.
14. Feybesse, J. L., Billa, M., Guerrot, C., Duguey, E., Lescuyer, J. L., Milési, J. P., & Bouchot, V. (2006). The Paleoproterozoic of the West African Craton: A synthesis. Precambrian Research, 149(3-4), 127–154.
15. Gasquet, D., Barbey, P., Adou, M., & Paquette, J. L. (2003). Geochronology, geochemistry and geodynamic significance of a Paleoproterozoic continental margin in the Baoulé-Mossi domain (West African Craton, Ivory Coast). Precambrian Research, 127(4), 313–329.
16. Gnanzou, A. (2014). Étude pétrographique et géochimique des granitoïdes de la région de Dabakala. Thèse de Doctorat, Université Félix Houphouët-Boigny, Abidjan, 210 p.
17. Hirdes, W., Davis, D. W., & Lüdtke, G. (1996). Two-stage Birimian (Paleoproterozoic) volcanism and plutonism in the West African Craton (Ghana) and their geodynamic significance. Precambrian Research, 80(3-4), 173–192.
18. Kouadio, K. J., Allou, Y., & Ouattara, A. S. (2023). Hydrothermal alteration and fluid evolution in Paleoproterozoic gold deposits of West Africa. Journal of African Earth Sciences, 198, 104780.
19. Kouamelan, A. N., Deloule, E., &Peucat, J. J. (1997). Geochronological and geochemical constraints on the Paleoproterozoic geological evolution of the Haute Côte d'Ivoire. Precambrian Research, 85(3-4), 183–202.
20. Lompo, M. (2009). Geodynamic evolution of the Paleoproterozoic Birimian formations of the Liptako-Gourma region (Eastern Burkina Faso). Journal of African Earth Sciences, 53(1-2), 45–60.
21. Martin, H., Smithies, R. H., Rapp, R., Moyen, J. F., & Champion, D. (2005). An overview of adakite, tonalite-trondhjemite-granodiorite (TTG) and sanukitoid: relationships and some implications for crustal evolution. Lithos, 79(1-2), 1–24.

22. Milési, J. P., Feybesse, J. L., Ledru, P., Dommanget, A., Marcoux, E., Egal, E., & Calvez, J. Y. (1989). Les minéralisations d'or du Birimien (Protérozoïqueinférieur) de l'Afrique de l'Ouest. Ses relations avec l'évolutionlithostructurale et géodynamique. Chronique de la Recherche Minière, 497, 3–58.
23. Reford, S. W. (2006). Airborne magnetic and gravity applications in mineral exploration. Geophysics, 71(6), G33–G47.
24. Siagné, Z. H., Ouattara, A. S., Konan, N. J. J., &Kouamé, F. (2022). New Lithostructural Map of the Doropo
25. Region, Northeast Côte d'Ivoire : Insight from Structural and Aeromagnetic Data. Journal of African Earth
26. Sciences, 196, 104680.
27. Siagné, Z. H., Ouattara, A. S., & Allou, Y. (2025). Integration of airborne gamma-ray spectrometry and remote sensing data for mapping of gold-bearing structures in the Doropo region, Northeastern Côte d'Ivoire. Geocarto International, 40(1), 2465074.
28. Tagini, B. (1971). Esquisse géologique de la Côte d'Ivoire: son rôle dans la structure géologique de l'Afrique de l'Ouest. Thèse de Doctorat, Univ. de Lausanne, 302 p.
29. Vidal, M., Deloule, E., Baratoux, L., & Jessell, M. W. (2009). Geodynamic evolution of the Birimian formations in Burkina Faso. Precambrian Research, 172(1-2), 110–128.